Journal of Geochemical Exploration 136 (2014) 1–13

Contents lists available at ScienceDirect

Journal of Geochemical Exploration

journal homepage: www.elsevier.com/locate/jgeoexp

Behavior of Zn-bearing phases in base metal slag from France and Poland: A mineralogical approach for environmental purposes

Maxime Vanaecker [a], Alexandra Courtin-Nomade [a,*], Hubert Bril [a], Jacky Laureyns [b], Jean-François Lenain [a]

[a] Université de Limoges, GRESE, E.A. 4330, IFR 145 GEIST, F.S.T., 123 Avenue A. Thomas, 87060 Limoges Cedex, France
[b] Université de Lille 1, USTL, LASIR, C5, BP 69, 59652 Villeneuve d'Ascq Cedex, France

ARTICLE INFO

Article history:
Received 18 February 2013
Accepted 3 September 2013
Available online 12 September 2013

Keywords:
Slag
Weathering
Zn-phase stability
Melilites
Raman spectroscopy

ABSTRACT

Slag samples from three pyrometallurgical sites (two in France, one in Poland) were studied for their Zn-phase content, evolution and potential release of metals over time. Mineral assemblages were observed and analyzed using various complementary tools and approaches: chemical extractions, optical microscopy, cathodoluminescence, X-ray diffraction, Scanning Electron Microscopy, Electron Probe Micro-Analysis, and micro-Raman spectrometry. The primary assemblages are composed of analogs to willemite, hardystonite, zincite, wurtzite, petedunnite and franklinite. Some of these phases are sensitive to alteration (e.g., deuteric processes during cooling and by weathering) and, as a result, goslarite, smithsonite and hemimorphite have been identified as secondary products. In comparing these results to the geochemical conditions at each site in relation to mineralogical investigations, different steps of Zn-rich mineral destabilization could be identified. This procedure allows assessing potential environmental impacts due to a release of metals that may contain slag. The destabilization of zincite leads to the precipitation of both goslarite and smithsonite, whereas only smithsonite is formed once hardystonite has been weathered. The Ca released by hardystonite dissolution will indeed limit goslarite formation and moreover favor gypsum precipitation. The relative degree of hydration necessary to form goslarite is supplied by water released during primary phase dissolution and/or smithsonite precipitation. A hydrated form of willemite was observed here, despite being rarely reported in previous studies, corresponding to an intermediate alteration product. The hydrated willemite ultimately evolved towards hemimorphite, which has been identified at the very outer part of the weathered willemite by means of EPMA and confocal Raman spectroscopy. On the basis of these results, we are able to propose a sequence from the least to most stable phase with: hardystonite and zincite > hemimorphite > willemite. Our results are critical for decisions like whether Zn-rich slag may be reused as a material for geotechnical purposes and thus contribute to the sustainable management of similar industrial wastes.

1. Introduction

During the 19th and 20th centuries, industrial development was linked to the activities of smelting plants that were treating large quantities of Zn–Pb and other base metal ores. Many countries in Europe engaged in such activities, and considerable amounts of wastes were in many cases abandoned in densely populated regions. Nowadays, these scattered dumpsites always contain up to several percent of Zn and other toxic metals and metalloids. The toxicity of these slag deposits has however been frequently overlooked; they are often indiscriminately considered as materials with limited reactivity and, due to their decent geotechnical properties, are regularly used for backfilling in urban areas, roadbeds, road ballast or as additives in the concrete industry (Barna et al., 2004; Bougaraa et al., 2010; De Angelis and Medici, 2012).

In Europe, the evolution of pyrometallurgical metal extraction methods over more than 200 years has resulted in large variations in the mineralogy, grain size, cooling processes and metal contents of such solid residues. The latest most efficient industrial processes allow recovering low metal concentrations, but typically lead to a finer particle size distribution of the residues, thereby facilitating interactions between solid phases and solutions. Even though the mineralogical assemblages remain comparable over time, the proportions of the various phases and total base metal content in these wastes vary considerably. This phenomenon can be illustrated by the differences between massive boulders still containing several percent of Zn and Pb, abandoned near smelting furnaces in industrial areas that had been in operation until the mid-20th century (De Andrade Lima and Bernardez, 2011; Peng et al., 2011), and the recent low Zn-grade glassy granulated slag that are relatively non-reactive (Knight and Henderson, 2006; Moustakas et al., 2012; Piatak and Seal, 2012).

Today's environmental concerns regarding waste residue, and especially slag from industrial activities, require detailed mineralogical investigations in order to assess their contamination potential into surface water seepage, groundwater and the food chain. Such an assessment is generally established after observing the behavior of specific samples

* Corresponding author. Tel.: +33 555 457 292; fax: +33 555 457 203.
E-mail address: alexandra.courtin@unilim.fr (A. Courtin-Nomade).

0375-6742/$ – see front matter © 2013 Elsevier B.V. All rights reserved.
http://dx.doi.org/10.1016/j.gexplo.2013.09.001

under laboratory conditions on the basis of leaching procedures that combine batch experiments and/or chemical extractions (sequential or selective) with geochemical codes (e.g., EQ3/6, Parsons et al., 2001; PHREEQC-2, Ettler et al., 2004; KindisP, Pareuil et al., 2010) for the purpose of simulating various environmental conditions as well as the potential release of metals from the host phases. Several authors have emphasized that these chemical approaches, such as sequential/selective extractions and their extrapolation to the entire contaminated area, are insufficient to assess the stability of metal host phases and may be supported by mineralogical investigations (Bril et al., 2008; Ettler et al., 2005, 2009; Piatak et al., 2004). This outcome has also been highlighted in numerous studies devoted to both primary and secondary assemblages subjected to conditions varying from slightly acidic to near-neutral (Navarro et al., 2008; Parsons et al., 2001; Piatak and Seal, 2010; Seignez et al., 2008), which are the conditions prevailing at our studied sites.

Based on previous detailed studies of both the mineralogical sequence of alteration (i.e., development of secondary phases) and batch experiments conducted on samples stemming from pyrometallurgical tailings present in three distinct European areas, this study is intended to: 1) compare the mineralogical assemblages in slag samples containing Zn-bearing phases; 2) infer the alteration potential of the main phases in the dumps, especially the Zn-host phases, when exposed to weathering under temperate climate conditions; 3) compare the assessment of long-term Zn mobility, as determined by mineralogical and chemical methods; and 4) improve the state of knowledge on the stability of some common Zn-bearing minerals, such as willemite (Zn_2SiO_4) and melilites $(Ca,Na)_2(Al,Mg,Fe)(Si,Al)_2O_7$, and on their reaction products under temperate climate conditions.

2. Materials and methods

2.1. Site and sampling description

The samples were collected from three former zinc smelters located in different climatic settings (Fig. 1). These three sites were chosen relative to the targeted operations and metallurgical processes as well as to potential contamination problems. About 10 samples were collected at each site, but only one unique sample displaying the most extensively developed alteration features will be presented herein for illustration purposes.

i. The "S" samples are from Upper Silesia (Świętochłowice, Poland), where the Zn smelter was active from 1858 through 1974. The wastes,

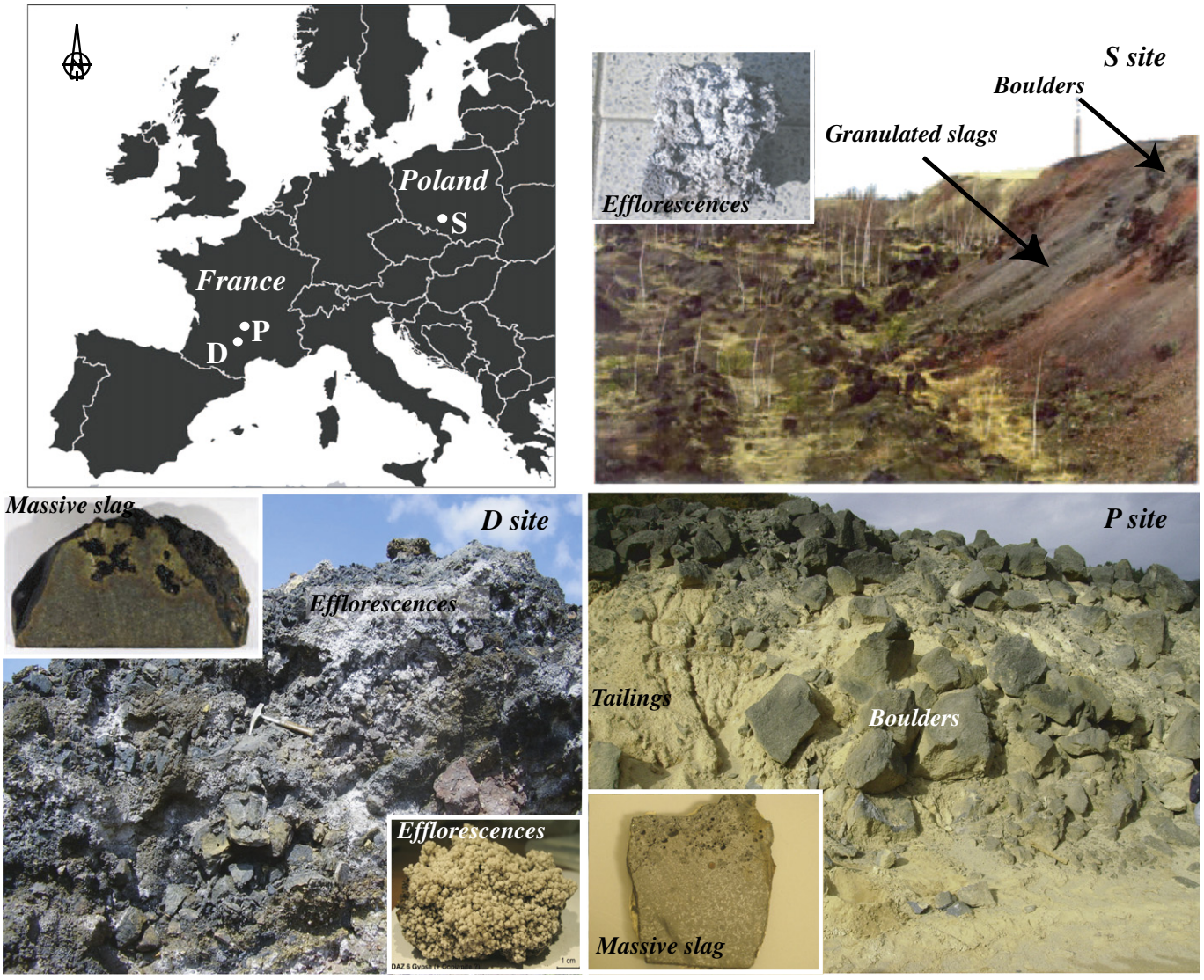

Fig. 1. General location map of the studied sites indicating the slag storage for each site and a representative image of the studied samples (D: Decazeville site; P: Pontgibaud site; S: Świętochłowice site).

still present on-site, are exposed to a cold and humid continental climate with an average temperature of 7.5 °C (seasonal averages: −1.7 °C in January and 17.7 °C in July) and subjected to acidic rainfall (a pH between 4 and 5 since 1991, Hlawiczka et al., 2003) that averages 750 mm per year (Bril et al., 2008; Puziewicz et al., 2007) (see Fig. 1, "S" site).

ii. The "D" samples originate from the Decazeville Basin (France), where the pyrometallurgical extraction of Zn ore remained active until 1922, when it was replaced by an industrial process based on the solubilization and electrolytic extraction of Zn that shut down in 1987 (Sivry et al., 2008). Cases of widespread contamination were reported in the Lot-Garonne river basin system by means of exposing various metallic elements, as highlighted by Audry et al. (2004, 2005, 2010) and Sivry et al. (2008). Even though some of these dumpsites were treated again using an electrolysis-based process between 1977 and 1987, As, Cd, Cu, Pb and Zn could still be detected: in non-smelting industrial wastes, at the watershed scale within the hydrographic system, and in soils, sediments and industrial wastes. The highest Zn concentrations measured by Sivry et al. (2008) were 639, 6687 and 56,262 mg · kg^{-1} respectively in soils, sediments and tailings. Audry et al. (2005) found 23 and 1190 μg L^{-1} of Cd and Zn respectively in the Riou-Mort, the stream running near the smelting plant. This contamination is due to leaching by rainwater of the metallurgical slag stored in dumps located along the river system (Fig. 1, "D" site). The climate here is oceanic, with an average annual temperature of 10.5 °C and rainfall of around 780 mm (http://france.meteofrance.com/france/climat_france).

iii. The "P" samples were collected in the Pontgibaud mining district (Massif Central, France), which is well known for lead and silver extraction and metallurgical processes that lasted centuries. Metallurgical activity continued until the very end of the 19th century (mainly from 1826 to 1897) using a Lead Blast Furnace-type process, though the initial ore was also rich in sphalerite. Since zinc was not being recovered at this site, the element is concentrated in the remaining slag (Fig. 1, "P" site). The dumps are exposed to a continental climate with an average annual temperature of 8.8 °C and rainfall of 892 mm (http://france.meteofrance.com/france/climat_france).

Due to the various origins and compositions of the mined ores and as a result of advances in Zn production technology, the wastes from these three sites reveal heterogeneous textures and mineralogical assemblages.

2.2. Analytical methods

2.2.1. Chemical composition and solid speciation

Bulk chemical analyses were performed by means of ICP-MS/ES at the ACME Analytical Laboratories (Vancouver, CAN) following lithium metaborate/tetraborate fusion and dilute nitric digestion, as well as at the SARM-CRPG Laboratory (Nancy, FR) in applying a similar protocol to that described above. Mineralogical assemblages within the slag samples were characterized by optical microscopy coupled with cathodoluminescence (CL) (i.e., a cooled cathode 8200 MKIV system, CITL Group, with a variable voltage of 8–27 kV and 200–800 mA, Laboratoire Géosystèmes, University of Lille 1, FR). This technique is able to highlight most of the stimulated Zn-phases because of their significant Mn content and moreover allows specifying the iron speciation in spinels. A spinel in fact reacts better under cathodoluminescence if it does not contain Fe^{2+} (an inhibitor) in its structure. X-ray diffraction (XRD), scanning electron microscopy equipped with an energy dispersive spectrometer system (SEM-EDS), electron microprobe (EPMA) and confocal Raman spectroscopy have all been carried out in order to discriminate the polymorphs developed as phases that sometimes overlap at the micro-scale. XRD analyses were performed using a Siemens D5000 diffractometer with CuK$\alpha_{1,2}$ radiation from 5° to 80° 2-theta at a rate of 0.12°2θ/min (SPCTS, University of Limoges, FR). The indexation and semi-quantification were obtained using X'pert Highscore Plus Panalytical software, which yields semi-quantification results based on both reference intensity ratios (RIR values) and the determined phase scale factors. Chemical composition analyses were conducted by both SEM-EDS (Philips XL 30, accelerating voltage of 20 kV, SerMiEl facility, University of Limoges, FR) and microprobe analyses (Camparis, University of Paris VI, FR). The microprobe (Cameca SX 50) operated at an accelerating voltage of 15 kV and a beam current of 4 nA. The standard reference materials used to calibrate quantitative analysis instruments are apatite, albite, orthoclase, galena, sphalerite, pyrite, diopside, pyrophanite, hematite, chromite, an AsGa alloy, tenorite and barite. The micro-Raman spectra were obtained at the L.A.S.I.R. Institute (UMR CNRS 8516, U.S.T.L. — Lille, FR) using two microspectrometers: one was a Labram Jobin Yvon (Horiba Group) with a He–Ne laser (632.8 nm), and the other a HoloLab Series 5000 (Kaiser Optical Systems) spectrometer coupled with an Invictus 785 nm NIR laser. The acquisition time ranged between 20 and 300 s, with an iteration number of 1, 2 or 3. The use of two lasers was specially indicated when a fluorescence phenomenon occurred. The power was set as low as possible (typically 1 mW) in order to prevent possible recrystallization from being induced by the beam, for instance (De Faria et al., 1997). The spectrum intensities, which depend on crystal orientation, are expressed in arbitrary units.

In the following section, mineralogical terminology will be used for the sake of clarity, even though synthetically-produced phases are not minerals according to the definition of the International Mineralogical Association (Nickel, 1995).

2.2.2. Leaching experiments

Leaching experiments were carried out on a representative sample from the sites of Decazeville ("D" site) and Pontgibaud ("P" site) on a polished section, whose 2 × 2 × 0.5 cm dimensions correspond to an 8-cm^2 contact surface area (contact between the solution and the downside surface has not been considered here), in order to obtain a solid/solution (S/V) ratio equal to 10 cm^{-1}. Since the results of tests performed on Polish samples had already been published by Bril et al. (2008), no further complementary leaching tests were carried out on the "S" samples. Three pH values were chosen for reactive solutions according to the protocol used by Ettler et al. (2002): 1) pH 3 was set with a sodium citrate/citric acid buffer solution to mimic an "organic soil" pH solution; 2) pH 5.5 was obtained using Milli-Q® deionized water; and 3) a solution saturated in $Ca(OH)_2$ generated a pH 12 so as to simulate the pH obtained in the case of lime remediation for neutralizing acidic conditions. Leaching experiments were performed for various time periods: 1 day, and 2, 5, 10, 20, 90, 120, 240, and 360 days. The pH and Eh values were measured at the end of each experimental time period. Leachate solutions were filtered to 0.45 μm prior to analysis by atomic absorption spectrometry (flame or furnace with a Varian SpectrAA660 and Varian SpectrAA 800 Zeeman, respectively) and anions by HPLC ionic chromatography (Dionex DX-100) at the GRESE Laboratory (Limoges, France). These analyses were duplicated and accuracy was measured at better than 15%.

3. Results

Decazeville samples show higher concentrations in Pb and Zn than Pontgibaud samples (Table 1). By being stored at high temperature as a liquid or viscous material, cooled dump material is often massive. Processes operated from 800 °C to 1320 °C under reducing conditions due to the addition of coke. Slag resulting from the cooling of Si–Ca melts can be massive or powdery, crystallized or glassy depending on the cooling rate (Gilchrist, 1989; Philibert et al., 2002). Glass however is rare in our samples given that the melts were not quenched by adding water (shot-blasting) at the end of metallurgical processes. Glass is only detected in heterogeneous powdery samples, such as D6 from the "D" area (Table 1, Fig. 2H).

Table 1
Bulk chemical compositions of the studied slags obtained by ICP-MS/ES (in % and mg/kg; n.d.: not determined) and mineralogical compositions as determined by bulk X-ray diffraction.

	Sample		D4	D6	S6	P1
	Texture		Massive well-crystalline	Powdery + efflorescences	High porosity	Massive well-crystalline
ICP	SiO_2	%	31.66	33.39	36.73	50.27
	Al_2O_3	%	10.31	10.56	9.09	16.9
	Fe_2O_3	%	16.90	12.63	17.00	10.33
	MgO	%	2.12	1.27	7.48	3.76
	CaO	%	30.24	16.42	18.49	7.2
	Na_2O	%	0.09	0.10	0.11	4.22
	K_2O	%	0.78	1.11	0.64	2.51
	TiO_2	%	0.39	0.41	0.45	1.97
	P_2O_5	%	0.27	0.20	0.17	0.87
	MnO	%	2.50	1.26	0.48	0.22
	LOI	%	0.24	13.78	5.88	1.3
	TOT/S	%	1.23	4.00	1.94	<0.02
	SUM	%	95.49	91.12	96.51	99.52
	Zn	%	1.66	2.45	0.75	0.01 mg/kg
	Pb	mg/kg	1400	28000	n.d.	1003
XRD	Akermanite		+			
	Franklinite		+			
	Pyrite		+			
	Hardystonite				+	+
	Wurtzite					+
	Lead					+
	Hyalophane					+
	Hemimorphite			+		
	Gypsum		+	+		
	Quartz		+	+		
	Petedunnite			+		
	Albite			+		
	Cristobalite			+		
	Tridymite			+		
	Willemite				+	
	Zincite				+	
	Magnetite			+		

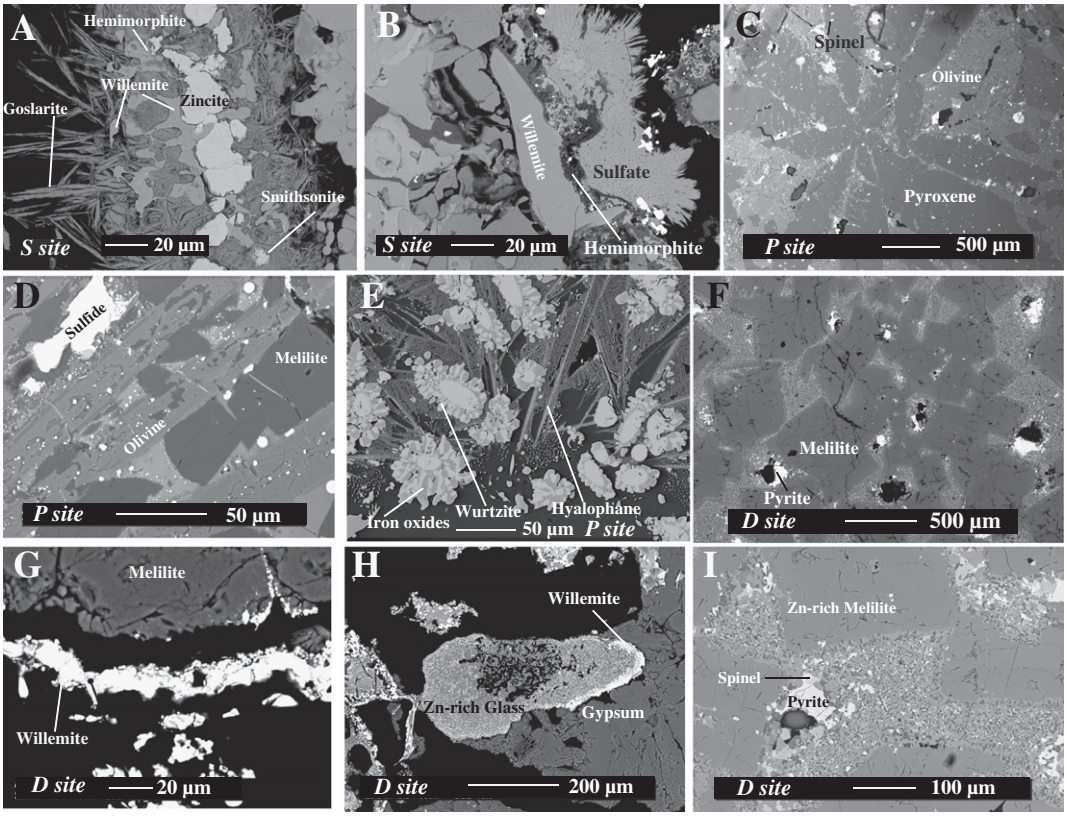

Fig. 2. Backscattered electron SEM photographs showing examples of texture and relationships between phases observed in samples from the S site (A and B), P site (C, D and E) and D site (F, G, H, I).

The slag samples studied display a wide variety of textures and mineralogy, including Ca, Mg or Fe silicates, oxides and sulfates. Only Zn-bearing phases however will be detailed herein. Despite varying Zn amounts, mineralogical and textural similarities were observed at the different sites, as previously reported by various authors, including Ettler et al. (2001), Parsons et al. (2001), Piatak and Seal (2010) and Thiry et al. (2002). Regarding the specific areas studied by these authors, silicates (willemite, melilites, zincian pyroxenes — $Ca(Zn,Mn^{2+},Fe^{2+},Mg)Si_2O_6$), sulfides (pyrite — FeS_2, wurtzite — (Zn,Fe)S) and oxides (zincite — ZnO, gahnite — $ZnAl_2O_4$ and franklinite — $Zn,Mn^{2+},Fe^{2+})(Fe^{3+},Mn^{3+})_2O_4$) are all present in the sample cores, although their proportions differ from one micro context to another (Fig. 2). Zn-sulfates, Zn-carbonates and iron (hydr-)oxides were identified in filling discontinuities, whereas Ca–Mg white-to-gray sulfate efflorescence coatings turn out to be frequent at the surface of materials across the range of sites (Fig. 1, "D" site). An example of the chemical composition of such efflorescence, observed on the surface of "D" samples, is provided in Table 1 (D6 sample) and indicates high contents in total sulfur, Pb and Zn.

The primary and secondary mineralogical assemblages will be described in detail in the following sections.

3.1. Primary Zn-bearing phases

Primary assemblages still represent the greatest percentage of material deposited as pyrometallurgical waste and thus the largest share of the studied samples. Despite being typically composed of silicates and oxides, these various assemblages and phase proportions are present to an extent that depends on melting and cooling conditions. For instance, assemblages observed in slag cores from Silesia and Pontgibaud are composed of zincian pyroxene and spinels (gahnite), revealing well-developed crystals (up to 5 mm in size) in vugs (Fig. 2C). At the border of these massive samples, the reported assemblages differ with willemite, melilites (hardystonite — $Ca_2ZnSi_2O_7$), quartz, spinels (franklinite) and zincite (Table 1, Fig. 2A, B, G and H).

Melilites $(Ca,Na)_2(Zn,Mg,Fe^{2+})[(Al,Si)SiO_7]$ are the most abundant phases, though their chemical composition varies from one site to the next (Table 2, Fig. 3). This mineral group presents a complete solid solution featuring hardystonite (Zn), containing up to 2% PbO, åkermanite (Mg) and ferro-åkermanite (Fe). The observed breadth of melilite composition is attributed to extraction processes: since Decazeville samples were less Zn-rich because Zn was the most widely recovered element, whereas Pontgibaud was mined for lead. The melilites observed are well developed, ranging from 1 to 10 mm in size (Fig. 3); they display an agpaitic or poecilitic texture with hyalophane inclusions and are commonly associated with sulfides (ferro-åkermanite with pyrite and hardystonite with wurtzite) and spinels, both of which are present in the matrix. Hardystonite crystals are indicated by a length-slow elongation, whereas other melilites are positive uniaxial, and crystals appear in green under cathodoluminescence stimulation. Moreover, an unusual pinkish pleochroism for ferro-åkermanite crystals ($FeCa_2Si_2O_7$) (Fig. 3) and a yellowish pleochroism for hardystonite crystals ($ZnCa_2Si_2O_7$) were noted, with identification being confirmed by XRD (e.g., Fig. 3). The two Raman spectra B1 and B2 presented in Fig. 4 were acquired on a melilite crystal (B1), which shows an alteration layer (B2) (see Fig. 4B for localization of the analyses). Raman spectra provide most of the characteristic bands of melilite (åkermanite and hardystonite), with the strongest bands at 661 cm^{-1} corresponding to the ν(Si–O–Si) ascribed to hardystonite and at 907 cm^{-1} to åkermanite (Fredericci et al., 2000; Sharma et al., 1988).

Willemite (Zn_2SiO_4) is present in samples from both Decazeville and Upper Silesia, in association with Zn-rich glass, franklinite, hardystonite and zincite (Fig. 2A and H). Willemite crystals up to 5 mm in size, presenting an unusual length-slow elongation and cleavages, are highlighted by franklinite inclusions in planes. Under cathodoluminescence, willemite crystals appear in very bright green (Fig. 4A) (Finch, 1990) due to the substitution of Zn by Mn in tetrahedral sites (El Ali et al., 1993). The willemites analyzed show extensive substitution of Zn by Mg (Table 2) and Mg-richer (8% MgO) cores with a continuously decreasing concentration at the borders. Two Raman spectra were obtained on willemite (A1

Table 2
Electron microprobe analyses of most representative observed Zn-bearing phases. Mole fractions of Fe^{2+} and Fe^{3+} were estimated by balance charge (**1**: Palache, 1935; **2**: Palache et al., 1944; **3**: Dana, 1892; **4**: Essene and Peacor, 1987; t.s.: this study; Ox.: number of normalized oxygen; NA: number of analyses).

	Willemite			Zincite		Hardystonite		Hemimorphite			Petedunnite		Franklinite		Gahnite	
	t.s.		1	t.s.	2	t.s.	1	t.s.		3	t. s.	4	t. s.	2	t. s.	2
SiO_2	28.74	29.16	*26.56*		*0.08*	36.31	*36.80*	24.88	24.92	*25.01*	41.74	*48.40*	0.74			*0.06*
Al_2O_3	0.39	0.04				0.62	*0.94*		1.03		5.17	*1.20*	8.89	*0.30*	55.48	*60.80*
TiO_2											0.28		0.66		0.23	
FeO	0.19	0.62	*0.81*	0.56	*0.01*	0.30	*0.20*	0.31	8.23		11.49	*5.70*			11.66	*12.09*
Fe_2O_3											0.00	*3.80*	56.58	*66.58*	5.29	
MnO	0.19	0.18	*8.96*		*0.27*		*0.76*	0.01	0.54		0.42	*5.80*	2.31	*6.60*	0.14	*0.46*
MgO	4.09	8.25	*1.05*	0.88		2.24	*0.39*		6.51		5.23	*2.40*	3.07	*0.30*	6.67	*0.46*
CaO			*0.75*			35.31	*34.61*		0.14		18.25	*21.30*				
BaO											0.20					
ZnO	**61.53**	**61.82**	**61.38**	**97.30**	**99.63**	**22.67**	**25.56**	**66.44**	**51.03**	**67.42**	**17.92**	**12.60**	**27.75**	**26.20**	**20.23**	**19.88**
Na_2O											0.28				0.15	
PbO			*0.01*			2.01	*0.56*	0.75	0.19		0.64	*0.70*				
Total	95.44	100.15	*99.74*	98.94	*99.99*	99.94	*100.11*	92.69	92.92	*93.27*	101.61	*101.90*	100	*100*	100	*100*
H_2O	4.6							7.31	7.08	*7.48*						
NA	7	15		12		8		6	5		4		18		6	
Ox.	4	4	*4*	1	*1*	7	*7*	10	10	*10*	6	*6*	4	*4*	4	*4*
Si	1.01	1.00	*0.97*			1.92	*1.94*	2.01	1.91	*2*	1.74	*1.94*	0.03			
Al		0.02				0.04	*0.06*		0.09		0.25	*0.06*	0.39	*0.01*	1.88	*2*
Ti											0.01		0.02			
Fe^{2+}	0.07	0.02	*0.02*	0.01		0.01	*0.01*	0.02	0.53		0.40	*0.19*			0.28	*0.28*
Fe^{3+}												*0.12*	1.57	*1.98*	0.11	
Mn	0.01	0.01	*0.28*				*0.03*		0.03		0.01	*0.20*	0.07	*0.22*		*0.01*
Mg	0.45	0.42	*0.06*	0.02		0.18	*0.03*		0.74		0.32	*0.14*	0.17	*0.02*	0.29	*0.30*
Zn	1.45	1.56	*1.66*	0.97	*0.99*	0.88	*1.00*	3.97	2.89	*3.99*	0.55	*0.37*	0.75	*0.77*	0.43	*0.41*
Ca			*0.03*			2.00	*1.96*				0.81	*0.92*				
Ba											0.003					
Pb						0.03	*0.01*	0			0.003					
Na											0.05	*0.06*				
Total	2.99	3.00	*3.03*	1	*1*	5.06	*5.03*	6.00	6.23	*5.99*	4.16	*4.00*	*2.99*	*3.00*	2.99	*3.00*

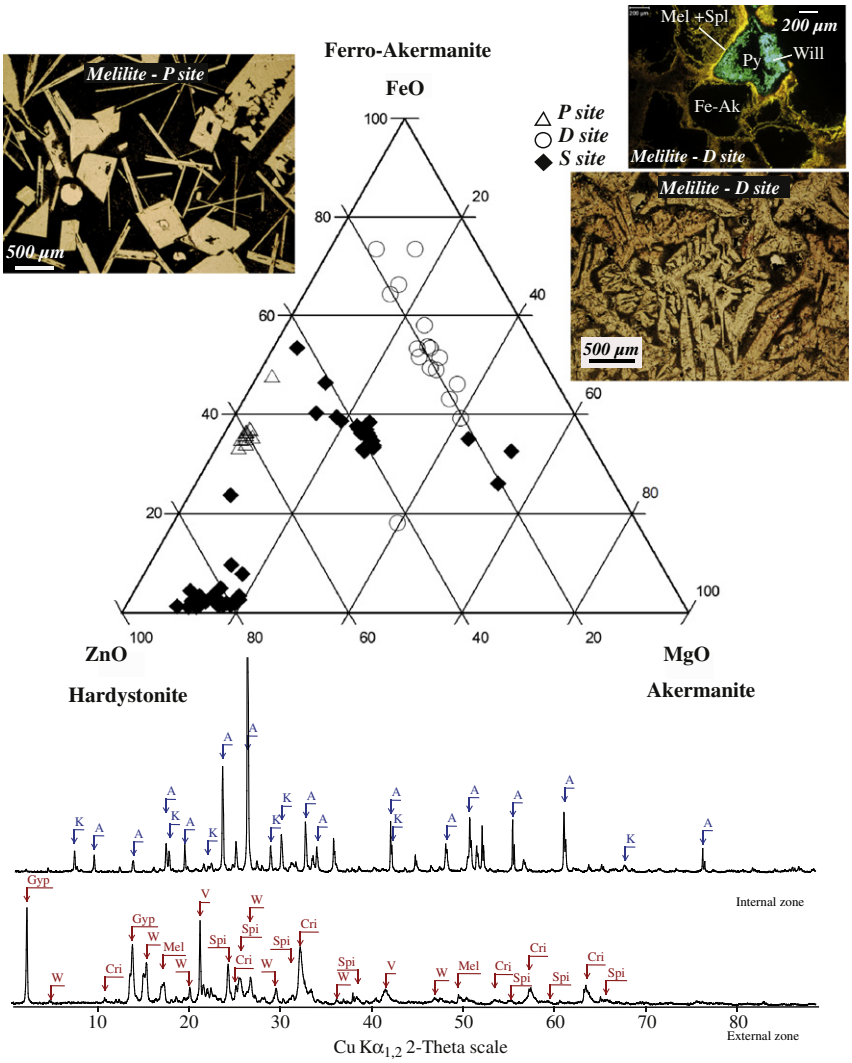

Fig. 3. ZnO–FeO–MgO ternary diagram of melilites in the three studied sites and optical microscopic images of melilites, hardystonites (top left) and ferro-åkermanites (bottom right) at the Pontgibaud (P1) and Decazeville (D4) sites, respectively. The top right image has been taken from cathodoluminescence on the D4 sample and successively displays: non-altered ferro-åkermanite (Fe–Ak, not cathodoluminescent); intergrowth with spinels (Spl) in yellow; willemite (Will) in green; and pyrite in the center (Py, not cathodoluminescent). The X-ray diffractograms confirm the presence of both primary and secondary phases at the center (internal zone) and border (external zone) of the D4 sample, with A: åkermanite and K: kirschsteinite Ca(Fe,Mn)SiO_4 for the internal zone, and Gyp: gypsum, W: willemite, Cri: cristobalite, Mel: melilite, V: vaterite ($CaCO_3$) and Spi: spinel for the external zone.

and A2, Fig. 4). Spectrum (A1) was acquired on a crystal core, while spectrum (A2) exhibits sharper peaks than (A1) along with broad bands between 2500 and 3200 cm^{-1} (see the inset in Fig. 4), corresponding to an OH stretching region (Frost and Bouzaid, 2007) that indicates hydration.

Zincite (ZnO) was detected in the "S" samples (Fig. 2A) by a bright green fluorescence under ultraviolet light (365 nm), coating the slag surfaces with a thickness of up to 1–2 cm. Zincite identification was confirmed by XRD (not shown here); however, the micro-Raman spectrum (C1) (Fig. 4) indicates that this phase is not pure zincite but rather a mix of zincite/Zn oxide. The spectrum indeed displays a distinct sharp band at 437 cm^{-1}, which is characteristic of Zn oxide (Baranov et al., 2005) plus weaker bands at 331, 378 and 409 cm^{-1}, indicative of zincite (Zn,Mn)O. The presence of "pure" zincite has furthermore been confirmed by the presence of a broad band at 526 cm^{-1} (Bouchard and Smith, 2003). Ultimately, zincite is not cathodoluminescent in our sample, thus indicating that Mn does not participate in this phase (El Ali et al., 1993).

Frequent in both slag (Ettler et al., 2001) and contaminated soils (Juillot et al., 2003), *spinels* are reported in almost all our samples, yet with a smaller size (up to 20 µm) than the other associated minerals (Fig. 2C and I). The most frequent one is franklinite ($ZnFe_2O_4$), which appears dark red in natural light and red under cathodoluminescence (Fig. 4A). This phase has been observed either in the matrix of samples or included in willemite cleavages. The chemical composition of spinels was determined by means of EPMA. The 100% sum for the spinel analyses in Table 2 is obtained after calculating the mole fraction of Fe^{2+} and Fe^{3+} by balance charge; the total measured amounted to 94.3% for franklinite and 99.4% for gahnite. Moreover, the red cathodoluminescence of franklinite underscores the absence of Fe^{2+} in its structure, which could have prevented the cathodoluminescence. Both Decazeville and Pontgibaud samples contain gahnite ($ZnAl_2O_4$), as detected by XRD and confocal Raman spectroscopy (not shown here), in association with pyroxenes in the inner part of the massive samples evidenced by green euhedral crystals.

Zn-rich pyroxenes (Ca(Zn,Mn^{2+},Fe^{2+},Mg)Si_2O_6) (~35%) were observed in the most inner part of the massive Pontgibaud samples with a composition close to that of petedunnite (Fig. 2C). Pyroxenes are good indicators of relatively slow cooling of the slag melt (Ettler et al., 2009). As determined by EPMA, Al and Zn in these pyroxenes are more abundant than in natural petedunnite (Table 2), as reported by Essene and Peacor (1987). Furthermore, this phase is widely associated

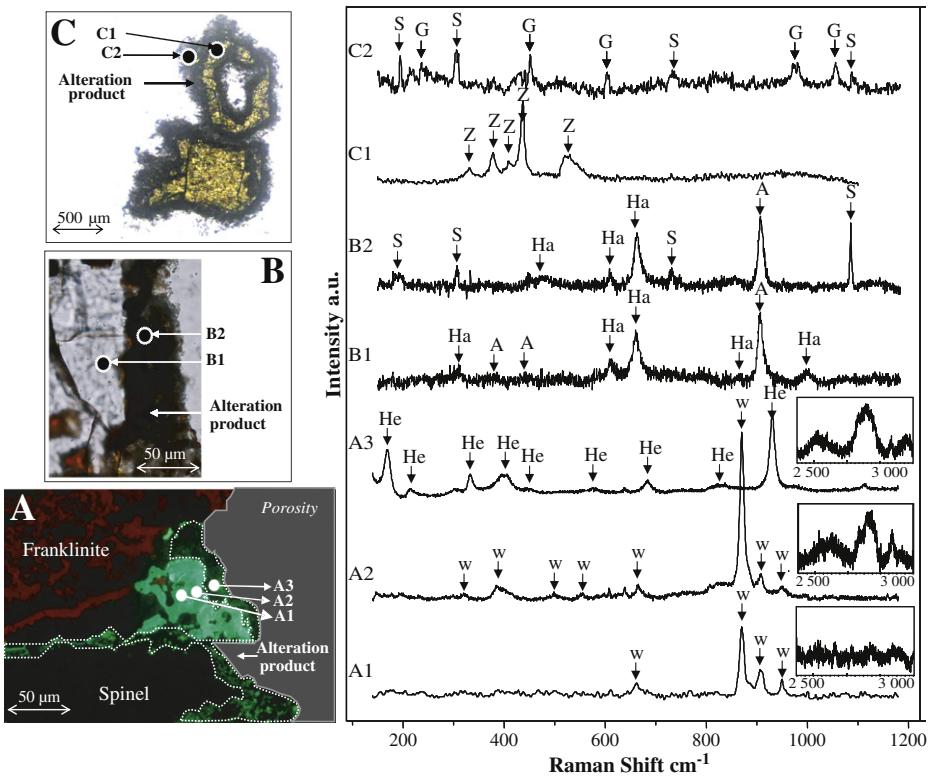

Fig. 4. Photographs of altered primary phases under A. cathodoluminescence and B. and C. optical microscope; A. willemite appears in very bright green, and its alteration product in pale green. The dark crystals on the photograph are spinels and franklinite appears in red; B. fresh melilites (B1) and a coating of secondary products on its border (B2); and C. altered zincite. The letters associated with black and white circles refer to the localization of Raman acquisitions with: A1. Willemite (W); A2. Hydrated willemite (see the 2500–3000 cm^{-1} region in the inset); A3. Hemimorphite (He); B1. Melilite: åkermanite (A) and hardystonite (Ha); B2. Melilite: hardystonite and smithsonite (S); C1. Zincite (Z); C2. Goslarite (G) and smithsonite.

with gahnite and contains, in addition to 5800 mg/kg Pb, more Zn and less Ca and Mn than "natural" petedunnite.

Rare *sulfides* have mainly been identified as wurtzite (~5% — (Zn,Fe)S) and pyrite (~10% — FeS_2). *Wurtzite* was detected in Pontgibaud samples associated with both petedunnite and hardystonite (Fig. 2D); it appears as fine crystals developed in cleavage planes of petedunnite but when associated with hardystonite, wurtzite is more developed and presents a botryoidal habit. Scanning electron microscopy analyses indicate intergrowths of Fe and Zn, thus suggesting the occurrence of an intimate mix of wurtzite with an Fe mineral specie, most probably wüstite (FeO), as previously reported by Seignez et al. (2007) in metallurgical waste from Northern France. *Pyrite* was identified within massive and crystalline samples from Decazeville, in association with spinels, as well as in the porosity near euhedral zincian melilites (Fig. 2F and I).

3.2. Secondary assemblages

In some cases, secondary phases are valuable host phases that allow trapping metals released after weathering processes; such phases are frequently observed in the studied slag samples and secondary assemblages can be identified according to their textural features: filling the fractures in massive samples, coating small-sized grains, filling vugs or dissolution cavities, an erratic and variable distribution throughout the sites, etc. (e.g., Seignez et al., 2008; Sobanska et al., 2000).

Always associated with willemite, *hemimorphite* $Zn_4Si_2O_7(OH)_2$ grows on its borders, where porosity is more developed (Figs. 2A, B and 4A). Hemimorphite is finely crystalline (1–30 µm) and presents a globular habit. Hemimorphite identification was supposed according to EPMA analyses, which show a higher degree of hydration (7 wt.% of H_2O) than willemite, and this finding was confirmed by confocal Raman spectroscopy. Two Raman spectra of willemite with well-defined peaks (A1 and A2) are presented in Fig. 3. Spectrum (A1) was acquired on a crystal core, while spectrum (A2) exhibits sharper peaks than (A1), though along with broad bands between 2500 and 3200 cm^{-1}, thus corresponding to an OH stretching region and indicating a hydrated form of willemite (Frost and Bouzaid, 2007). Spectrum (A3), obtained at the edge of the willemite crystal, differs from the two previous spectra, which indicates that it is no longer willemite but instead hemimorphite with the broad bands in the OH stretching region (Fig. 4). The bands at 164, 331, 394, 451, 543, 676, 869, 1114 cm^{-1} and the strongest band at 929 cm^{-1} are all ascribed to hemimorphite (Frost et al., 2007; Kolesov, 2006). The chemical compositions of the analyzed hemimorphites suggest variations in both Fe (up to 8 wt.%) and Mg (up to 6 wt.%) contents (Table 2). The presence of Fe, which acts as an inhibitor, combined with the absence of Mn explains the lack of cathodoluminescence properties typically observed for hemimorphite (Fig. 4A).

Goslarite $ZnSO_4$ and *smithsonite* $ZnCO_3$ appear as intergrowths of micrometric crystals on zincite borders. Confocal Raman spectroscopy allows identifying these two mineral species, although their chemical composition is difficult to determine due to their small size and intergrowths (Fig. 4C). Moreover, smithsonite solely forms 50-µm thick coatings on hardystonite (Fig. 4B) and was identified by confocal Raman spectroscopy, with characteristic bands being reported (Fig. 4, spectra B2 and C2). When altered, zincite crystals are replaced by fine needles of authigenic sulfates (Figs. 2A and 4C), and this replacement proves to be most effective in cleavage planes.

3.3. Leaching experiments

Massive and well-crystalline slag samples D4 ("D" site) and P1 ("P" site) were chosen for their high melilite content. The aim of these

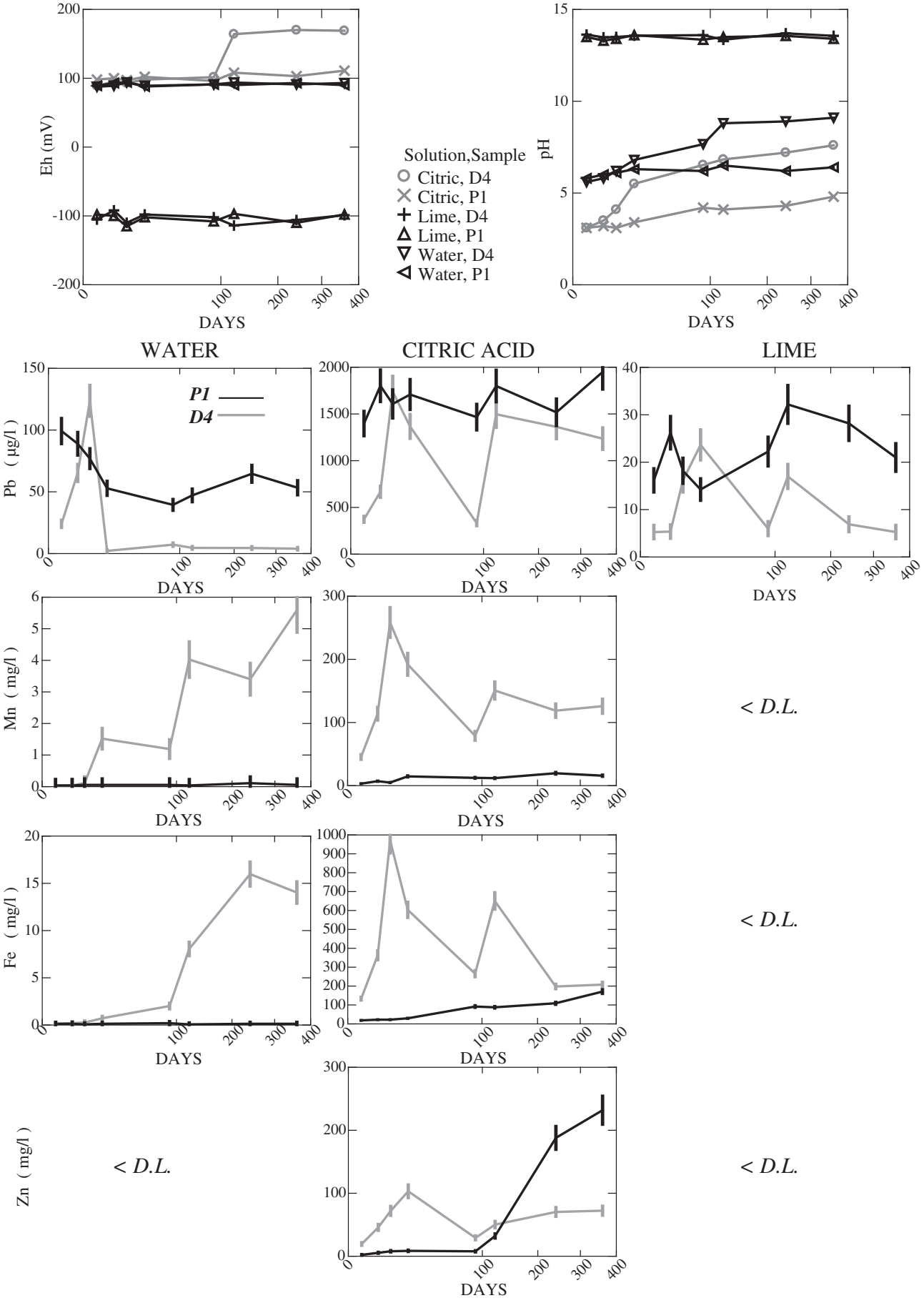
Eh (mV)
DAYS
Solution,Sample
Citric, D4
Citric, P1
Lime, D4
Lime, P1
Water, D4
Water, P1
pH
DAYS
WATER
CITRIC ACID
LIME
P1
D4
Pb (µg/l)
DAYS
Mn (mg/l)
< D.L.
Fe (mg/l)
< D.L.
Zn (mg/l)
< D.L.

leaching experiments was to compare two melilite–sulfide systems among the most abundant and richest minerals in Zn: the Decazeville system (D4) was saturated in Fe (the semi-quantification from XRD analyses yields 86% of ferro-åkermanite containing around 3% Zn, 8% franklinite and 6% pyrite), whereas the Pontgibaud system (P1) was saturated in Zn (with semi-quantification results of 72% hardystonite, 16% wurtzite, 8% Ba-rich feldspars, plus droplets of elemental lead also noticed).

3.3.1. Lime medium

At high pH values, the two systems were totally inert, as indicated by no modification to the physicochemical parameters (Eh and pH) and no detectable Zn in the dissolved fraction (Fig. 5). Despite low concentrations of the analyzed metals, it is worthwhile to notice that when placed in contact with lime (which could be used for remediation purposes), Pb can be remobilized regardless of the sample (Fig. 5).

3.3.2. Citric acid medium

In acidic and complexing media, both samples presented high reactivity. Eh and pH evolved similarly in both cases even though D4 seems to be the more reactive sample (i.e., a higher increase in pH values) compared to P1 (Fig. 5). pH values increased from an initial pH 3 to 7.2 and 4.3 for D4 and P1, respectively; Eh values remained similar throughout the experiment for P1, i.e., around 100 mV, whereas a significant increase in Eh was observed after 90 days for D4 (90 mV and 170 mV at the beginning and end of the experiment, respectively). During these experiments, Pb and Zn were more mobilized in P1 (P1: $C_{Pb\_360d} = 2000\ \mu g\ L^{-1}$; P1: $C_{Zn\_360d} = 250\ mg\ L^{-1}$) in comparison with D4 ($C_{Pb\_360d} = 1250\ \mu g\ L^{-1}$; $C_{Zn\_360d} = 75\ mg\ L^{-1}$); for a single element however, a similar trend can be observed between the two samples. Fe and Mn concentrations were higher in D4, which might be due to the higher primary content of these elements in this sample as they both displayed a similar trend for the same sample. It may also be noted that Mn was only released in the citric acid medium. Eventually, at 90 days and only for the D4 sample, a drop in the concentrations of every analyzed element was observed simultaneously with a jump in the Eh value (Fig. 5).

Surface observations of the two samples, as summarized in Table 3, reveal different alteration features. The D4 sample surface shows the precipitation of white to yellowish globular crystals, corresponding to calcium citrate (as identified by IR; not shown here) formed during the first 5 days of the experiment, along with alteration features on the melilites (Fig. 6, A2, A3). The ferro-åkermanites tend to be depleted in Ca, Fe and Zn at the expense of Si after the experiment has run 20 days, with the formation of amorphous silica gel that develops more extensively over time. An X-ray elemental map obtained after 120 days highlights this dissolution of melilites, and a thin layer of amorphous silica can be seen at the alteration front (Fig. 6B). Despite concentrations in the dissolved fraction of 1250 $\mu g\ L^{-1}$ Pb and 75 $mg\ L^{-1}$ Zn after a year, the globular crystals function as efficient sinks for Pb and Zn, with 2.7 and 4.5 wt.% measured respectively after 360 days of the experiment (the initial Pb concentration in melilites was on average 0.1%). Surface observations of the P1 sample pointed out the high alteration of hardystonite surfaces, which occurred progressively during the experiment, but the globular crystals of calcium citrates were only detected after 360 days (Fig. 6, C1).

3.3.3. Water medium

The variations in pH values suggest that D4 was affected in contact with water while no measurable variation was observed for the P1 sample (around 6) (Fig. 5). A modification to the pH value at 90 days (almost 1 unit of pH) was noted for D4, occurring at the same time as the increase in Fe and Mn concentrations (Fig. 5). After 90 days, the pH reached a stable value of around 9 (Fig. 5), with concentrations remaining low however: up to 16 $mg\ L^{-1}$ for Fe and 6 $mg\ L^{-1}$ for Mn, and no Zn was measured in the dissolved fraction regardless of the sample (Fig. 5). Following a jump in Pb concentrations to 120 $\mu g\ L^{-1}$, these values rapidly decreased to the detection threshold after 20 days (Fig. 5). Analyses of the dissolved P1 sample fraction indicated no release of Fe, Mn or Zn (Fig. 5). Lead was detected in the dissolved fraction at 100 $\mu g\ L^{-1}$ after one day, but its concentration decreased progressively to reach a steady state at around 50 $\mu g\ L^{-1}$ between the 90th and 360th day (Fig. 5). No alteration feature in the P1 sample surface was detected following the leaching experiment whenever small holes could be observed in place of the pyrites within the D4 sample (Fig. 6, A1; Table 3).

4. Discussion

The frequent presence of secondary phases indicates that the studied sites are sources of metallic elements, which implies that slag is not as inert as generally considered. The presence of minerals with obvious secondary characteristics does not however provide any indication of the temporal lag separating the crystallization of primary phases and the formation of secondary ones. In other words, phases characterized as secondary can be formed either during the cooling of slag ("deuteric" phases), or as a byproduct of ore roasting (Piatak and Seal, 2010), or from low temperature phases as a result of weathering processes. These secondary phases are thus more abundant when dump permeability is enhanced by various processes, such as cooling-induced cracks and fractures created during handling. Nonetheless, this study has shed some light on the alteration pathway of the main primary phases – willemite, melilites and zincite – and moreover may help assess the stability of the identified authigenic products.

4.1. Destabilization of hardystonite

Melilites occur in Ca-saturated environments, as naturally observed in skarns (Pascal et al., 2001) or ultramafic magmas (Akal, 2003; Di Battistini et al., 2001). Melilites are known to be pseudomorphically replaced in skarns by vesuvianite ($Ca_{10}Mg_2Al_4(SiO_4)_5(Si_2O_7)_2(OH)_4$) and cebollite ($Ca_5Al_2(SiO_4)_3(OH)_4$) (Joesten, 1974; Pascal et al., 2001). The mineralogical occurrences of such phases under supergene conditions however require complementary data. Several previous studies (Di Battistini et al., 2001; Ettler et al., 2002) indicated that melilite alteration is characterized by a significant release of Ca, Mg and Mn. Melilite alteration into submicrometer nepheline ($(Na,K)AlSiO_4$) and pyroxenes has mainly been documented in the case of chondrites exposed to aqueous conditions only present in asteroidal settings (e.g., Lin and Kimura, 1998; Wasson et al., 2001). Under supergene conditions, weathering has not been well documented: only Kucha et al. (1996) observed significant dissolution of melilites in an acidic solution (pH 2), although these authors also pointed out that melilites are among the most resistant minerals regardless of the studied solution pH. Furthermore, under natural conditions, Kierczak et al. (2009) noticed that melilites were not affected by weathering. In the studied samples, smithsonite develops on hardystonite crystals, yet no association with either goslarite or zincite was observed. Gypsum, the most abundant alteration product in our samples, was identified in some pores close to melilites, suggesting that other sulfates and carbonates may be similarly associated with melilites. The abundance of gypsum indicates a Ca-saturated system, and melilite dissolution provides a portion of the Ca necessary for gypsum

Fig. 5. pH and Eh evolution and concentration variations of Zn, Fe, Mn (in $mg\ L^{-1}$) and Pb (in $\mu g\ L^{-1}$) throughout the leaching experiments, which lasted 360 days on samples D4 and P1 in the three solutions (water, lime and citric acid; D.L.: detection limit).

Table 3
Leaching experiment summary of the observations of the sample surfaces after 360 days in the three different solutions.

Media			
Sample	Citric acid	Water	Lime
D4 *Ferro-åkermanite*	Highly altered surface with geometrical corrosion figures of former melilites	Slight alteration of the surface except some sulfides released during the experiments	No visible alteration
P1 *Hardystonite*	Altered surface with geometrical corrosion figures of former melilites	No alteration	No visible alteration

formation, in agreement with Di Battistini et al. (2001). The dissolution reaction may be written as follows:

$$Ca_2ZnSi_2O_7 + H_2O + 6H^+ \leftrightarrow 2Ca^{2+} + Zn^{2+} + 2H_4SiO_{4(aq)}. \quad (1)$$

According to reaction (1), the dissolution of hardystonite tends to increase Ca activity in the solution by releasing twice as much Ca as Zn. The absence of goslarite is therefore due to a preferential precipitation of gypsum, in consuming SO_4^{2-} ions, that increases the activities of both HCO_3^- and Zn^{2+} and then allows smithsonite to precipitate.

Furthermore, leaching experiments provide an assessment of the relative reactivities and stabilities of the ferro-åkermanite and hardystonite present in our samples (Table 3). Hardystonite appears to be more resistant to alteration processes than ferro-åkermanite, which implies a lower mobility of Zn compared to Fe. This observation agrees with the presence of Fe(II) in the tetrahedral position into ferro-åkermanites (or within pyrite), which consequently favors its oxidation and allows destabilization of the crystal lattice as well as the release of associated minor elements. We did observe similar behavior between Fe and Mn, thus suggesting the same origin and similar kinetics of the release.

4.2. Formation of hemimorphite by willemite hydration

Willemite is an orthosilicate of Zn typically observed in hypogene deposits (Borg et al., 2003; Groves et al., 2003) and frequently formed

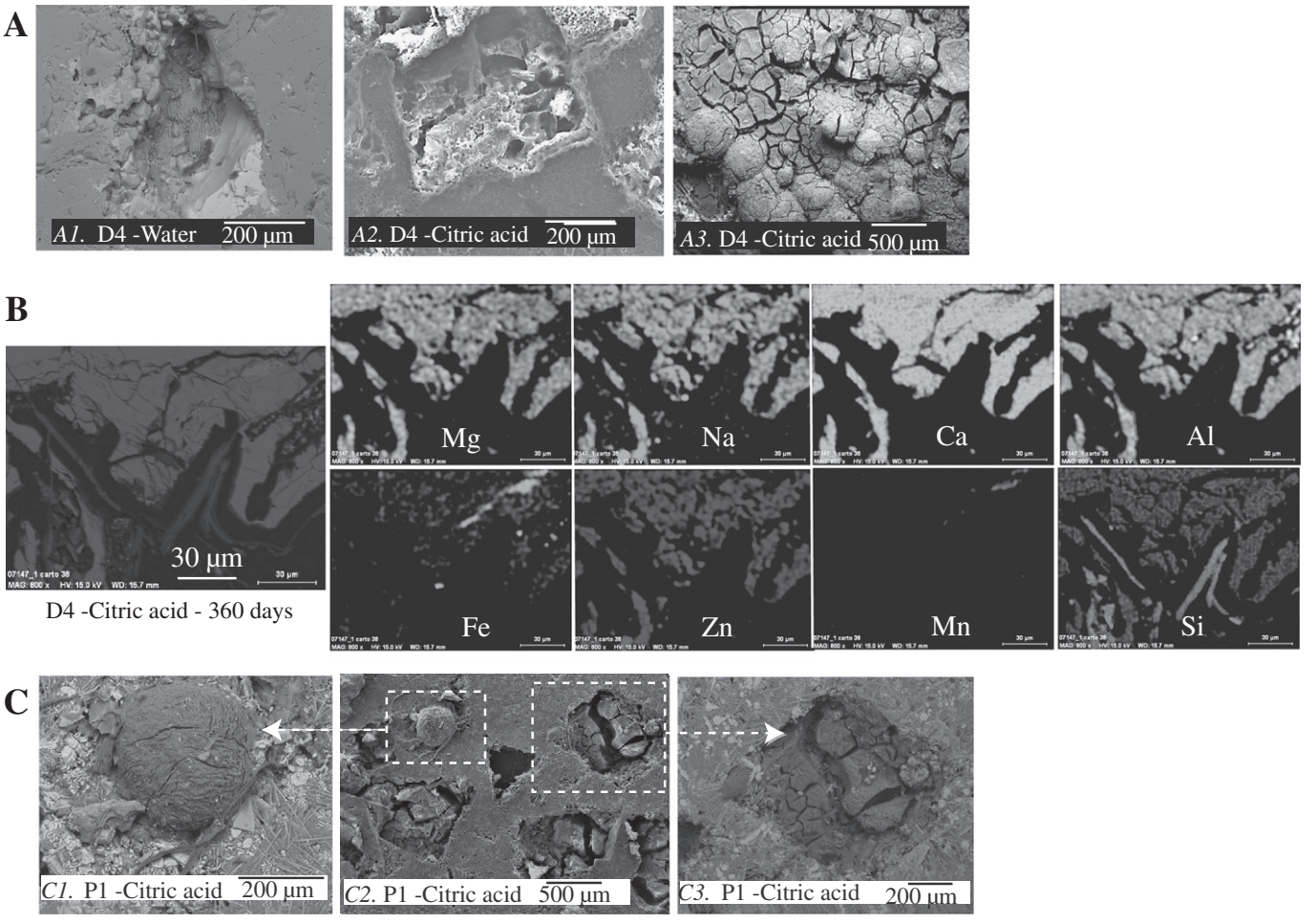

Fig. 6. Alteration features observed on D4 and P1 samples after leaching experiments with A./A1. SEM image of D4 after 360 days in a water solution showing alteration features of the sulfides (light gray at the bottom right of the photograph); A2. SEM image of the D4 sample after 20 days in a citric acid solution showing the alteration of a melilite grain; A3. SEM image of the silica gel and globular precipitates of calcium citrate developed on the surface of the D4 sample after 360 days in a citric acid solution; B./SEM X-ray elemental distribution of the main components of the amorphous silica gel on the D4 sample after 360 days in the citric acid solution; C./P1 surface sample after 360 days in the citric acid solution and alteration features observed with SEM as C1. Newly formed globular precipitates of calcium citrate; C2. Overview of the surface sample; and C3. Altered melilite.

under hydrothermal conditions (Brugger et al., 2003; Hitzman et al., 2003). Its association with hemimorphite is frequent (Hitzman et al., 2003), notably under supergene conditions (e.g., Boni et al., 2009), although reactions leading to the crystallization of hemimorphite remain poorly understood (Coppola et al., 2008, 2009). Hemimorphite may then lead to Zn–smectite (sauconite — $Na_{0.3}Zn_3(Si,Al)_4O_{10}(OH)_2 \cdot 4(H_2O)$) alteration products (Boni et al., 2009).

In the studied samples, the textural relationship suggests that hemimorphite stems from willemite destabilization and its formation may be induced by willemite hydration (Fig. 2A and B). Such a reaction has rarely been considered, although the opposite reaction of a hemimorphite-to-willemite transformation was reported by Roy and Mumpton (1956) and Liu et al. (2005), who synthesized willemite after hemimorphite dehydration. In our samples, confocal Raman spectroscopy allows identifying an intermediate hydrated phase between willemite and hemimorphite that displays a lower Mg content (4%) than the willemite cores. This progressive hydration of willemite from the core to the border is confirmed by the increasing intensity of the Raman spectra bands between 2500 cm^{-1} and 3000 cm^{-1} (Fig. 4, spectra A1 to A3).

A study on the vibrational dynamics in H^+ substituted forsterite by Shaw and Tse (2007) revealed that O – H bonds are preferentially located in M1 sites, as characterized by peaks occurring in the region between 700 and 1200 cm^{-1} and around 2800 cm^{-1} on calculated IR spectra. In the studied willemites, observed bands between 2500 cm^{-1} and 3000 cm^{-1} on Raman spectra suggest a similar configuration to the O – H bonds in M1 sites of willemite. The exchange of H^+ with Mg^{2+} during forsterite alteration had already been reported by Pokrovsky and Schott (2000) and Wilson (2004). These authors considered such an exchange as the precursor mechanism of iddingsitization. As regards willemite alteration, the hydration of willemite by Mg^{2+} substitution may also be considered as a precursor of hemimorphite formation. An argument supporting this hypothesis is the presence of Mg in hemimorphite. Below 850 °C, Mg is metastable in willemite and then preferentially integrated into hemimorphite (Libowitzky and Rossman, 1997; Palache et al., 1944). In comparing this reaction with iddingsite formation (Greenwood et al., 2000; Smith et al., 1987), fluid generation during cooling generates a metastable hydrated willemite, which evolves into hemimorphite by weathering, as favored by the presence of aqueous silica in weathering fluids. The transformation of willemite into hemimorphite could then be described as follows:

Mg^{2+}/H^+ exchange: deuteric (hydrothermal) alteration stage

$$(Zn_{1.5}Mg_{0.5})SiO_4 + \alpha H_2O \leftrightarrow Zn_{1.5}SiO_4 \cdot \alpha H_2O + 0.5Mg^{2+} \quad (2)$$

Formation of hemimorphite incorporating Mg: weathering (supergene) stage

$$2Zn_2SiO_4 \cdot \alpha H_2O_{(unstable)} + (2-\alpha)H_2O + \beta Mg^{2+} \leftrightarrow (Zn_{(4-\beta)}Mg_\beta)Si_2O_7(OH)_2 \cdot H_2O. \quad (3)$$

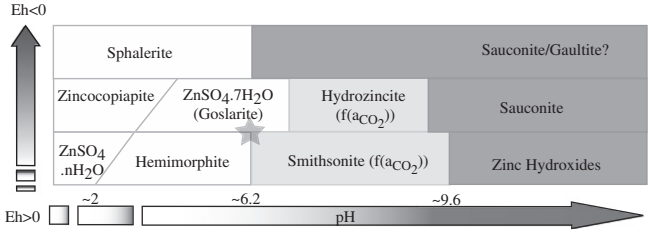

Fig. 7. Conceptual diagram for the Eh–pH stability conditions for some of the observed Zn-bearing phases.

4.3. Destabilization of zincite

According to Bénézeth et al. (1999) and Wesolowski et al. (1998), zincite is stable in a neutral to alkaline solution and destabilized under acidic conditions (Fig. 7), as expressed in the following reaction (4).

$$ZnO + 2H^+ \leftrightarrow Zn^{2+} + H_2O. \quad (4)$$

Zincite is the latest primary phase formed during the cooling and its high sensitivity to weathering is enhanced by direct exposure to runoff. The observed secondary products are a 500-μm to 2-mm thick coating the zincite surface, corresponding to a mixture of smithsonite and goslarite. Hales and Frost (2007) described smithsonite formation as a function of CO_2 pressure by the following reactions:

$$5Zn^{2+}_{(sol)} + 10HCO_3^-(sol) \leftrightarrow Zn_5(CO_3)_2(OH)_{6(s)}(hydrozincite) + 8CO_{2(g)} + 2H_2O \quad (5a)$$

(modified from Hales and Frost, 2007)

$$Zn_5(CO_3)_2(OH)_{6(s)} + 3CO_{2(g)} \leftrightarrow 5ZnCO_{3(s)}(smithsonite) + 3H_2O \quad (5b)$$

(Hales and Frost, 2007)

$$Zn^{2+}_{(sol)} + 2HCO_3^-(sol) \leftrightarrow ZnCO_{3(s)} + CO_{2(g)} + H_2O \quad (6)$$

(modified from Hales and Frost, 2007).

These reactions imply high CO_2 activity. The absence of hydrozincite relics is supported by reaction (6). Regardless of the reaction, the presence of HCO_3^- and CO_2 is necessary to form smithsonite and moreover indicates an acidic to neutral environment, in agreement with zincite dissolution and the sometimes concomitant goslarite formation (Jambor et al., 2000). Furthermore, according to Chou and Seal (2005), the presence of goslarite is only possible at high relative humidity (>42%), in agreement with all of the cited reactions. Goslarite ($ZnSO_4 \cdot 7H_2O$) may indeed retain water following the dissolution of zincite and thus inhibit the formation of hydrozincite, in accordance with reactions (7a) and (7b):

$$ZnO + H_2SO_4 \leftrightarrow Zn^{2+} + SO_4^{2-} + H_2O \quad (7a)$$

$$Zn^{2+} + SO_4^{2-} + nH_2O \leftrightarrow ZnSO_4 \cdot (n)H_2O. \quad (7b)$$

The stability of the various Zn-phases within the slag samples will depend on two main parameters: slag porosity, and the intrinsic properties of the considered phases. The less stable slag samples are either powdery or the most porous, thereby facilitating contact with the solution. Alteration features have been observed for every primary phase either as a result of in situ alteration or due to processes occurring during the leaching experiments. Only olivine and pyroxene were not altered, as their location enabled preservation in the massive sample core and thus no exposure, for instance, to meteoric runoff.

The leaching experiments also highlight that the main problem related to slag is not Zn but rather other trace elements, especially Pb, even though the concentrations remained relatively low (with a maximum of 1800 μg L^{-1} measured for acidic conditions). Lead measured in the leachates is not explained in terms of mineralogical origin but, as mentioned previously, is correlated with the partial destabilization of the main bearing phases listed in Table 2, such as melilites and Zn-rich pyroxenes.

Among the primary phases, some are more sensitive to alteration (spinels for instance remain unaltered as predicted), and authigenic products such as goslarite, smithsonite and hemimorphite may form under supergene conditions. Fig. 7 shows the prevailing Eh/pH conditions for the formation of some of the Zn-species identified herein. Goslarite and smithsonite result from the destabilization of zincite

when the supergene alteration of hardystonite leads only to the formation of smithsonite. This outcome may be explained by the fact that calcium from hardystonite dissolution would limit the formation of goslarite at the expense of gypsum. The water content necessary to form goslarite is supplied by the dissolution of primary phases and/or the precipitation of smithsonite. Among the identified authigenic products, a hydrated form of willemite was found to eventually evolve into hemimorphite located at the outer part of the hydrated willemite, as confirmed by EPMA and μ-Raman analyses. The formation of hemimorphite is initiated by the substitution of Mg^{2+} with H^{+} in willemite during the deuteric alteration, which is fully achieved under supergene conditions.

5. Conclusion

The present study has offered a thorough characterization of the alteration of Zn-rich phases commonly associated with dumpsites abandoned by pyrometallurgical industries, in focusing herein on temperate climates and low to medium rainfall regimes. We have found evidence for the alteration of phases reputed to be resistant and have concluded that nearly all primary Zn-rich phases identified in our samples were unstable under supergene conditions, over a wide range of pH conditions (except spinels). The studied samples have been slightly altered however due to their generally massive state as well as to an increasing alteration reaction rate whenever water penetration is favored. In contrast, modern granulation processes should increase the potential hazard of these residues as a result of the small size of particles left at the dumpsite even though the concentrations of hazardous elements are lower in more recent slag thanks to technological improvements in recovering smaller concentrations. Nevertheless, the main difference between mine tailings and slag residues is that the tailings are sulfide-rich materials and crushed to the mm scale (or more frequently the μm scale), thus representing a more concentrated source of pollution.

In addition, slag surfaces may be coated with authigenic and more soluble phases, such as sulfate efflorescence, which are able to dissolve during rain events. As an example among the most unstable phases, the weathering of zincite leads to the formation of smithonite and goslarite, in forming a thick layer of secondary crystals on the zincite surface, as suggested by the reaction (5b) of smithsonite formation (however, this mineral is only stable under high CO_2 partial pressures). Willemite and melilites also present alteration features, but to a lesser extent, with smithsonite observed growing on hardystonite and hemimorphite on willemite. Calcium leached from the alteration of hardystonite also leads to the formation of gypsum along with smithsonite. Hemimorphite formation is hard to decipher between its deuteric (hydrothermal) and supergene origins, but Raman analyses suggest that hemimorphite formation is enhanced by the hydration of willemite.

This study has emphasized that the reactions relative to Zn-bearing primary silicates and common oxides in metallurgical waste, as summarized in Fig. 7 and hereafter, are actually possible due to weathering:

$$\text{Hardystonite} \leftrightarrow \text{Smithonite} + \text{Gypsum}$$

$$ZnCa_2Si_2O_7 + H_2O + CO_2 + H^+ \leftrightarrow ZnCO_3 + 2Ca^{2+} + 2H_4SiO_4$$

$$2Ca^{2+} + 2SO_4^{2-} + H_2O \leftrightarrow CaSO_4 \cdot 2H_2O$$

$$\text{Zincite} \leftrightarrow \text{Goslarite} + \text{Smithsonite}$$

$$ZnO + H_2SO_4 + CO_2 + 6H_2O \leftrightarrow ZnSO_4 \cdot 7H_2O + ZnCO_3$$

$$\text{Hemimorphite} \leftrightarrow \text{Goslarite}$$

$$Zn_4Si_2O_7(OH)_2 \cdot H_2O + 4H_2SO_4 + 22H_2O \leftrightarrow 4(ZnSO_4 \cdot 7H_2O) + 2SiO_2$$

$$\text{Willemite} \leftrightarrow \text{Hemimorphite}$$

$$2Zn_2SiO_4 + 2H_2O \leftrightarrow Zn_4Si_2O_7(OH)_2 \cdot H_2O.$$

Among the studied phases, a sequence from least to most stable can be proposed:

hardystonite and zincite > hemimorphite > willemite.

This conclusion should be taken into account in the context of recycling Zn-bearing slag both for geotechnical tasks and for a sustainable management of industrial wastes.

Acknowledgments

This work has been supported by the Limousin Regional Council (France). The authors would like to thank Professors G. Blanc (University of Bordeaux, UMR CNRS 5805) and S. Audry (University of Toulouse, UMR CNRS 5563) for their assistance in sampling, S. Gouy and P. Recourt (University of Lille 1, UMR 8110), Mathieu Daëron (LSCE, Gif-sur-Yvette) and D. Proust (University of Poitiers, UMR 6532,) for their overall collaboration.

References

Akal, C., 2003. Mineralogy and geochemistry of melilite leucitites, Balçikhisar, Afyon (Turkey). Turk. J. Earth Sci. 12, 215–239.
Audry, S., Schäfer, J., Blanc, G., Jouanneau, J.-M., 2004. Fifty-year sedimentary record of heavy metal pollution (Cd, Zn, Cu, Pb) in the Lot River reservoirs (France). Environ. Pollut. 132, 413–426.
Audry, S., Blanc, G., Schäfer, J., 2005. The impact of sulphide oxidation on dissolved metal (Cd, Zn, Cu, Cr, Co, Ni, U) inputs into the Lot-Garonne fluvial system (France). Appl. Geochem. 20, 919–931.
Audry, S., Grosbois, C., Bril, H., Schäfer, J., Kierczak, J., Blanc, G., 2010. Post-depositional redistribution of trace metals in reservoir sediments of a mining/smelting-impacted watershed (the Lot River, SW France). Appl. Geochem. 25, 778–794.
Baranov, A.N., Solozhenko, V.L., Château, C., Bocquillon, G., Petitet, J.P., Panin, G.N., Wang, T.W., Shpanchenko, R.V., Antipov, E.V., Oh, Y.J., 2005. Cubic MgxZn1-xO wide band gap solid solutions synthesized at high pressures. J. Phys. Condens. Matter 17, 3377–3384.
Barna, R., Moszkowicz, P., Gervais, C., 2004. Leaching assessment of road materials containing primary lead and zinc slags. Waste Manage. 24, 945–955.
Bénézeth, P., Palmer, D.A., Wesolowski, D.J., 1999. The solubility of zinc in 0.03 m NaTr as a function of temperature, with in situ pH measurement. Geochim. Cosmochim. Acta 63, 1571–1586.
Boni, M., Balassone, G., Arseneau, Vernon, Schmidt, Paul, 2009. The nonsulfide zinc deposit at accha (Southern Peru): geological and mineralogical characterization. Econ. Geol. 104, 267–289.
Borg, G., Kärner, K., Buxton, M., Armstrong, R., Van der Merwe, S.W., 2003. Geology of the Skorpion supergene zinc deposit, Southern Namibia. Econ. Geol. 98, 749–771.
Bouchard, M., Smith, D.C., 2003. Catalogue of 45 reference Raman spectra of minerals concerning research in art history or archaeology, especially on corroded metals and coloured glass. Spectrochim. Acta A Mol. Biomol. Spectrosc. 59, 2247–2266.
Bougaraa, A., Lynsdaleb, C., Milestonec, N.B., 2010. Reactivity and performance of blast furnace slags of differing origin. Cem. Concr. Compos. 32, 319–324.
Bril, H., Zainoun, K., Puziewicz, J., Courtin-Nomade, A., Vanaecker, M., Bollinger, J.C., 2008. Secondary phases from the alteration of a pile of zinc-smelting slag as indicators of environmental conditions: an example from Świętochłowice, Upper Silesia, Poland. Can. Mineral. 46, 1235–1248.
Brugger, J., McPhail, D.C., Wallace, M., Waters, J., 2003. Formation of willemite in hydrothermal environments. Econ. Geol. 98, 819–835.
Chou, I.-M., Seal II, R.R., 2005. Determination of goslarite–bianchite equilibria by the humidity-buffer technique at 0.1 MPa. Chem. Geol. 215, 517–523.
Coppola, V., Boni, M., Gilg, H.A., Balassone, G., Dejonghe, L., 2008. The "calamine" nonsulfide Zn–Pb deposits of Belgium: petrographical, mineralogical and geochemical characterization. Ore Geol. Rev. 33, 187–210.

Coppola, V., Boni, M., Gilg, A.H., Strzelska-Smakowska, B., 2009. Nonsulfide zinc deposits in the Silesia–Cracow district, Southern Poland. Miner. Deposita 44, 559–580.

Dana, E.S., 1892. Dana's System of Mineralogy, 6th edition. John Wiley & Sons, New York 546–549.

De Andrade Lima, L.R.P., Bernardez, L.A., 2011. Characterization of the lead smelter slag in Santo Amaro, Bahia, Brazil. J. Hazard. Mater. 189, 692–699.

De Angelis, G., Medici, F., 2012. Reuse of slags containing lead and zinc as aggregate in a Portland Cement matrix. J. Solid Waste Technol. Manag. 38, 117–123.

De Faria, D.L.A., Venancio Silva, S., De Oliveira, M.T., 1997. Raman microspectroscopy of some iron oxides and oxyhydroxides. J. Raman Spectrosc. 28, 873–878.

Di Battistini, G., Montanini, A., Vernia, L., Venturelli, G., Tonarini, S., 2001. Petrology of melilite-bearing rocks from the Montefiascone Volcanic Complex (Roman Magmatic Province. New insights into the ultrapotassic volcanism of Central Italy. Lithos 59, 1–24.

El Ali, A., Barbin, V., Calas, G., Cervelle, B., Ramseyer, K., Bouroulec, J., 1993. Mn^{2+}-activated luminescence in dolomite, calcite and magnesite. quantitative determination of manganese and site distribution by EPR and CL spectroscopy. Chem. Geol. 104, 189–202.

Essene, E.J., Peacor, D.R., 1987. Petedunnite (CaZnSi2O6), a new clinopyroxene from Franklin, New Jersey, and phase equilibria with for zincian pyroxenes. Am. Mineral. 72, 157–166.

Ettler, V., Mihaljevic, M., Touray, J.-C., 2001. Metallurgical slag behavior in extreme conditions. Surface Leaching and Metal Mobility ENSMP. Mémoire des Sciences de la Terre, 40 81–83.

Ettler, V., Mihaljevic, M., Touray, J.-C., Piantone, P., 2002. Leaching of polished sections. An integrated approach for studying the liberation of heavy metals from lead–zinc metallurgical slags. Bull. Soc. Geol. Fr. 173, 161–169.

Ettler, V., Komárková, M., Jehlička, J., Coufal, P., Hradil, D., Machovič, V., Delorme, F., 2004. Leaching of lead metallurgical slag in citric solutions — implications for disposal and weathering in soil environments. Chemosphere 57, 567–577.

Ettler, V., Mihaljevič, M., Šebek, O., Strnad, L., 2005. Leaching of APC residues from secondary Pb metallurgy using single extraction tests: the mineralogical and the geochemical approach. J. Hazard. Mater. B121, 149–157.

Ettler, V., Červinka, R., Johan, Z., 2009. Mineralogy of medieval slags from lead and silver smelting (Bohutín, Příbram district, Czech Republic): towards estimation of historical smelting conditions. Archaeometry 51, 987–1007.

Finch, A.A., 1990. Genthelvite and willemite, zinc minerals associated with alkaline magmatism from the Motzfeldt centre, South Greenland. Mineral. Mag. 54, 407–412.

Fredericci, C., Zanotto, E.D., Ziemath, E.C., 2000. Crystallization mechanism and properties of a blast furnace slag glass. J. Non-Cryst. Solids 273, 64–75.

Frost, R.L., Bouzaid, J.M., 2007. Raman spectroscopy of dawsonite $NaAl(CO_3(OH_2)$. J. Raman Spectrosc. 38, 873–879.

Frost, R.L., Bouzaid, J.M., Jagannadha Reddy, B., 2007. Vibrational spectroscopy of the sorosilicate mineral hemimorphite $Zn_4(OH)\ 2Si_2O_7 \cdot H_2O$. Polyhedron 26, 2405–2412.

Gilchrist, J.D., 1989. Extraction Metallurgy, 3rd edition. Pergamon press, Oxford, U.K.

Greenwood, J.P., Riciputi, L.R., McSween Jr., H.Y., Taylor, L.A., 2000. Modified sulfur isotopic compositions of sulfides in the nakhlites and Chassigny. Geochim. Cosmochim. Acta 64, 121–1131.

Groves, I.M., Carman, C.E., Dunlap, W.J., 2003. Geology of the Beltana willemite deposit, Flinders Ranges, South Australia. Econ. Geol. 98, 797–818.

Hales, M.C., Frost, R.L., 2007. Synthesis and vibrational spectroscopic characterisation of synthetic hydrozincite and smithsonite. Polyhedron 26, 4955–4962.

Hitzman, M.W., Reynolds, N.A., Sangster, D.F., Allen, C.R., Carman, C.E., 2003. Classification, genesis and exploration guides for nonsulfide zinc deposits. Econ. Geol. 98, 685–714.

Hlawiczka, S., Dyduch, B., Fudala, J., 2003. Long-term changes of particulate emission in the industrial region of upper Silesia (Poland) and their effect on the acidity of rainwater. Water Air Soil Pollut. 142, 151–163.

http://france.meteofrance.com/france/climat_france.

Jambor, J.L., Nordstrom, D.K., Alpers, C.N., 2000. Metal–sulfate salts from sulfide oxidation. Rev. Mineral. 40, 303–350.

Joesten, R., 1974. Pseudomorphic replacement of melilite by idocrase in a zoned calc-silicate skarn. Christmas Mountains, Big Bend Region, Texas. Am. Mineral. 59, 694–699.

Juillot, F., Morin, G., Ildefonse, P., Trainor, T.P., Benedetti, M., Galoisy, L., Calas, G., Brown, G.E., 2003. Occurrence of Zn/Al hydrotalcite in smelter-impacted soils from northern France. Evidence from EXAFS spectroscopy and chemical extractions. Am. Mineral. 88, 509–526.

Kierczak, J., Néel, C., Puziewicz, J., Bril, H., 2009. The mineralogy and weathering of slag produced by the smelting of lateritic ni ores, Szklary, Southwestern Poland. Can. Mineral. 47, 557–572.

Knight, R.D., Henderson, P.J., 2006. Smelter dust in humus around Rouyn-Noranda, Québec. Geochem.: Explor. Environ., Anal. 6, 203–214.

Kolesov, B., 2006. Raman investigation of H_2O molecule and hydroxyl groups in the channels of hemimorphite. Am. Mineral. 91, 1355–1362.

Kucha, H., Martens, A., Ottenburgs, R., De Vos, W., Viaene, W., 1996. Primary minerals of Zn–Pb mining and metallurgical dumps and their environmental behavior at Plombières, Belgium. Environ. Geol. 27, 1–15.

Libowitzky, E., Rossman, G.R., 1997. IR spectroscopy of hemimorphite between 82 and 373 K and optical evidence for a low-temperature phase transition. Eur. J. Mineral. 9, 793–802.

Lin, Y., Kimura, M., 1998. Anorthite-spinel-rich inclusions in the Ningqiang carbonaceous chondrite: genetic links with type A and C inclusions. Meteorit. Planet. Sci. 33, 435–446.

Liu, Y., Deng, J., Yang, L.Q., Wang, Q.F., 2005. The dehydration of hemimorphite. Acta Petrol. Sin. 21, 993–998.

Moustakas, K., Mavropoulos, Al, Katsou, E., Haralambous, K.-J., Loizidou, M., 2012. Leaching properties of slag generated by a gasification/vitrification unit: the role of pH, particle size, contact time and cooling method used. J. Hazard. Mater. 207–208, 44–50.

Navarro, A., Cardellach, E., Mendoza, J.L., Corbella, M., Domènech, L.M., 2008. Metal mobilization from base-metal smelting slag dumps in Sierra Almagrera (Almería, Spain). Appl. Geochem. 23, 895–913.

Nickel, E.H., 1995. The definition of mineral. Can. Mineral. 33, 689–690.

Palache, C., 1935. The minerals of Franklin and Sterling Hill, Sussex County, New Jersey. U.S. Geological Survey, Prof. Paper 180.

Palache, C., Berman, H., Frondel, C., 1944. 7th edition. Dana's System of Mineralogy, 1 504–506.

Pareuil, P., Bordas, F., Joussein, E., Vieillard, P., Bollinger, J.-C., 2010. Leaching experiments on a Mn-rich slag from the recycling of alkaline batteries — solid phase characterization and geochemical modeling. Appl. Geochem. 25, 1187–1197.

Parsons, M.B., Bird, D.K., Einaudi, M.T., Alpers, C.N., 2001. Geochemical and mineralogical controls on trace element release from the Penn Mine base-metal slag dump, California. Appl. Geochem. 16, 1567–1593.

Pascal, M.-L., Fonteilles, M., Verkaeren, J., Piret, R., Marincea, S., 2001. The melilite-bearing high-temperature skarns of the Apuseni Mountains, Carpathians, Romania. Can. Mineral. 39, 1405–1434.

Peng, X., Jiao, B., Li, D., 2011. Heavy metal's potential harm for environment of ancient pyrometallurgical slag. Adv. Mater. Res. 160–162, 130–134.

Philibert, J., Vigne, A., Brechet, Y., Combrade, P., 2002. Métallurgie: du minerai au matériau, 2nd edition. Dunod, Paris.

Piatak, N.M., Seal II, R.R., 2010. Mineralogy and the release of trace elements from slag from the Hegeler Zinc smelter, Illinois (USA). Appl. Geochem. 25, 302–320.

Piatak, N.M., Seal, R.R., 2012. Mineralogy and environmental geochemistry of historical iron slag, Hopewell Furnace National Historic Site, Pennsylvania, USA. Appl. Geochem. 27, 623–643.

Piatak, N.M., Seal II, R.R., Hammarstrom, J.M., 2004. Mineralogical and geochemical controls on the release of trace elements from slag produced by base- and precious-metal smelting at abandoned mine sites. Appl. Geochem. 19, 1039–1064.

Pokrovsky, O.S., Schott, J., 2000. Kinetics and mechanism of forsterite dissolution at 25 °C and pH from 1 to 12. Geochim. Cosmochim. Acta 64, 3313–3325.

Puziewicz, J., Zainoun, K., Bril, H., 2007. Primary phases in pyrometallurgical slags from a zinc smelting waste dump, Świętochłowice, Upper Silesia, Poland. Can. Mineral. 45, 1333–1344.

Roy, D.M., Mumpton, F.A., 1956. Stability of minerals in the system $ZnO–SiO_2–H_2O$. Econ. Geol. 51, 432–443.

Seignez, N., Bulteel, D., Buatier, M., Recourt, P., Damidot, D., Potdevin, J.L., 2007. Effect of Pb-rich and Fe-rich entities during alteration of a partially vitrified metallurgical waste. J. Hazard. Mater. 149, 418–431.

Seignez, N., Gauthier, A., Bulteel, D., Damidot, D., Potdevin, J.-L., 2008. Leaching of lead metallurgical slags and pollutant mobility far from equilibrium conditions. Appl. Geochem. 23, 3699–3711.

Sharma, S.K., Yoder Jr., H.S., Matson, D.W., 1988. Raman study of some melilites in crystalline and glassy states. Geochim. Cosmochim. Acta 52, 1961–1967.

Shaw, D.M., Tse, J.S., 2007. Vibrational dynamics in H + -substituted forsterite. A first-principles molecular dynamics study. Am. Mineral. 92, 1593–1600.

Sivry, Y., Riotte, J., Sonke, J.E., Audry, S., Schäfer, J., Viers, J., Blanc, G., Dupré, B., 2008. Zn isotopes as tracers of anthropogenic pollution from Zn–ore smelters The Riou Mort–Lot River system. Chem. Geol. 255, 295–304.

Smith, K.L., Milnes, A.R., Eggleton, R.A., 1987. Weathering of basalt: formation of iddingsite. Clays Clay Miner. 35, 418–428.

Sobanska, S., Ledésert, B., Deneele, D., Laboudigue, A., 2000. Alteration in soils of slag particles resulting from lead smelting. C.R. Acad. Sci., Ser. IIa: Sci. Terre Planets 331, 271–278.

Thiry, M., Huet-Taillanter, S., Schmitt, M., 2002. La friche industrielle de Mortagne-du-Nord 59. Prospection du site, composition des scories, hydrochimie, hydrogéologie et estimation des flux. Bull. Soc. Geol. Fr. 173, 359–369.

Wasson, J.T., Yurimoto, H., Russell, S.S., 2001. ^{16}O-rich melilite in CO3.0 chondrites: possible formation of common, ^{16}O-poor melilite by aqueous alteration. Geochim. Cosmochim. Acta 65, 4539–4549.

Wesolowski, D.J., Bénézeth, P., Palmer, D.A., 1998. ZnO solubility and Zn^{2+} complexation by chloride and sulfate in acidic solutions to 290 °C with in-situ pH measurement. Geochim. Cosmochim. Acta 62, 971–984.

Wilson, M.J., 2004. Weathering of the primary rock-forming minerals. Processes, products and rates. Clay Miner. 39, 233–266.